Enhanced Rotation by Ground State Destabilization in Amphidynamic Crystals of a Dipolar 2,3-difluorophenylene Rotator as Established by Solid State ^{2}H NMR and Dielectric Spectroscopy

Ieva Liepuoniute,[1] Chau Minh Huynh,[1,2] Salvador Perez-Estrada,[1,3] Yangyang Wang,[4] Saeed Khan,[1] K. N. Houk[1] and Miguel A. Garcia-Garibay[1]*

[1]Department of Chemistry and Biochemistry, University of California, Los Angeles, California 90095-1569, USA

[2]Umeå University, Department of Chemistry, S-90187 Umeå, Sweden

[3]Área Académica de Química, Centro de Investigaciones Químicas, Universidad Autónoma del Estado de Hidalgo, Ciudad del Conocimiento, Hidalgo 42184, México

[4] Center for Nanophase Materials Sciences, Oak Ridge National Laboratory, Oak Ridge, Tennessee 37831, USA

ABSTRACT: We report the synthesis and rotational dynamics of the pillared metal organic framework $Zn_2(F_2BDC)_2(DABCO)$ where F_2BDC=2,3-difluorobenzene-1,4-dicarboxylate acts as a rotating dipolar linker and DABCO=1,4-diazabicyclo[2.2.2]octane as a spacer (F_2MOF **1**). The pillared structure of F_2MOF **1** was confirmed by X-ray diffraction and CP-MAS ^{13}C NMR analyses. Using variable temperature solid state ^{2}H NMR and broadband dielectric spectroscopy, we characterized the rotational dynamics of the dipolar F_2BDC linker in the solid state. Variable temperature (VT) quadrupolar echo ^{2}H NMR measurements revealed a rotational activation energy of E_a = 6.8 ± 0.1 kcal/mol, which agreed well with temperature and frequency-dependent dielectric measurements, indicating a barrier of E_a = 7.1 ± 0.5 kcal/mol. Structural data from single crystal X-ray diffraction and quantum mechanical calculations (DFT) suggest that the rotational potential is determined by steric interactions between the dipolar rotator and the stator linkers such that fluorine atoms in the F_2BDC linker reduce the activation energy by destabilization of the coplanar BDC ground state.

INTRODUCTION

Amphidynamic crystals are built with a combination of static, lattice-forming elements that are linked to mobile molecular components.[1-4] The most promising approach for the realization of amphidynamic crystals is based on the design of crystalline molecular rotors.[1-6] These materials have attracted a great deal of attention because they are expected to provide opportunities to control many of their physical properties by collectively changing the dynamics and orientation of dipolar rotators as they interact with each other and with external fields.[1-4,7,8] To optimize the desired behavior, it is important to increase the magnitude of the dipole-dipole interactions (E_{DD}) to the point that they are greater than thermal energy (kT) and rotational barriers (Ea). Amphidynamic materials with E_{DD} >> kT ≥ Ea are expected to exhibit spontaneous order with dipolar arrays being susceptible to external switching to control their ferroelectric, acoustic and optical properties.[3,9-11] With this goal in mind, we explored the dynamics of the dipolar fluorophenylene[12] and 2,3-difluorophenylene[13] rotators axially attached by alkyne axles to triphenylmethyl stators. However, the densely packed environments of their corresponding molecular crystals led to large barriers to rotation (13.7 and 14.1 kcal/mol, respectively), which prevented the observation of dipolarly-ordered phases.

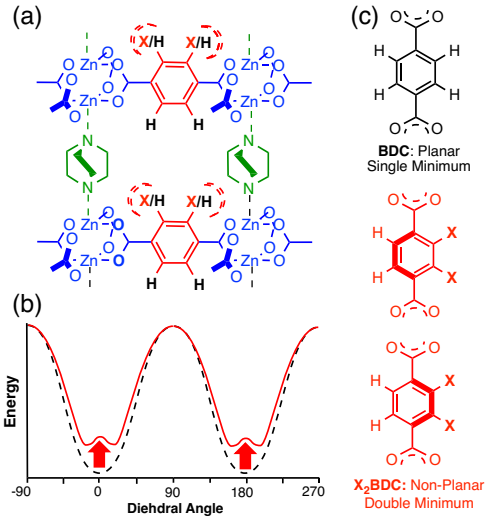

Figure 1. (a) $Zn_2(H_4/X_2BDC)_2(DABCO)$ MOF structure. (b) Expected potential energy diagrams for BDC (dashed black line) and X_2BDC rotation (solid red line), and (c) the corresponding line structures of BDC and X_2BDC. Steric interactions between the *ortho* X-substituent and the carboxylate group destabilize the ground state in the polar X_2BDC.

As an alternative to densely packed molecular crystals, and seeking to generate 2D square grids of closely interacting dipolar rotors, we have now prepared crystals of the pillared MOF $Zn_2(F_2BDC)_2(DABCO)$ (F_2MOF **1**, F_2BDC=2,3-difluorobenzene 1,4-dicarboxylate, DABCO=1,4-diazabicyclo[2.2.2]octane) featuring the dipolar F_2BDC rotator (Figure 1a, X=F). We selected the F_2BDC linker because of its small size and reasonably large dipole moment of μ≈3.0 Debye.[13] DABCO was selected as the spacer between layers of $[Zn_2(F_2BDC)_2]$ because of its proven ability to form pillared MOFs. In fact, isomorphous pillared MOFs with unsubstituted benzene dicarboxylate $Zn_2(BDC)_2(DABCO)$ (H_4MOF **2**),[14] and the tetrafluorobenzene dicarboxylate $Zn_2(F_4BDC)_2(DABCO)$ (F_4MOF **3**, F_4BDC=2,3,5,6-tetrafluorobenzene-dicarboxylate)[15] have been reported in the literature. Furthermore, crystal structures of the F_4BDC rotator in F_4MOF **3** and a similar BrBDC rotator in the zinc oxide cluster-containing IRMOF-2 $[Zn_4(C_6H_3O_4\text{-}Br)_3]$ are characterized by disordered aromatic rings that avoid co-planarity with the carboxylate,[16] suggesting that steric or electrostatic interactions between the aryl substituents and the carboxylate oxygens destabilize the otherwise co-planar ground state minimum (Figure 1b).[17] Based on that, we hypothesize that the barrier to rotation for F_2MOF **1** should be lower than that of H_4MOF **2**, as suggested by the red solid potential in Figure 1b. The local maximum is postulated to occur due to the steep rise in van der Waals repulsion when atoms come closer than their van der Waals radii. Using variable temperature quadrupolar echo ^{2}H NMR and temperature and frequency dependent dielectric spectroscopy to measure the rotational motion of F_2BDC linker we confirmed that fluorine substitution reduces the activation energy from E_a = 8.6 kcal/mol in the non-polar H_4MOF **2**[14] to E_a = 6.8 kcal/mol in F_2MOF **1**. We also report computational results that provide us with some insight into the energy changes that affect the rotational potential.

Scheme 1

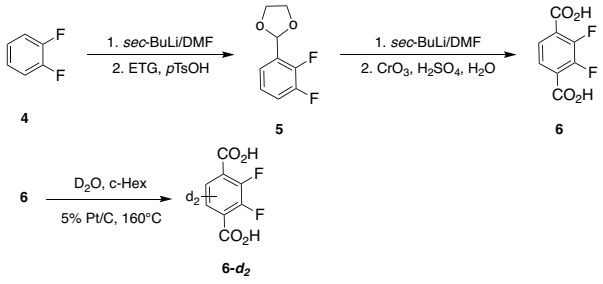

ETG: ethylene glycol

RESULTS AND DISCUSSION

Synthesis, Thermal Analysis and Crystal Structures. The F_2BDC linker **6** was prepared in four steps from 1,2-difluorobenzene **4**. As shown in Scheme 1, the synthesis started with lithiation of **4** by treatment with *sec*-butyllithium, followed by reaction with *N,N*-dimethylformamide (DMF) and protection of the resulting aldehyde as a dioxolane to afford compound **5**. The ligand F_2BDC **6** was obtained by formylation of **5** *via* lithiation followed by deprotection and oxidation of the dialdehyde using Jones reagent (Scheme 1). The deuterium isotopologue **6-*d*$_2$** was obtained by heating at 160 °C in a sealed pressure vessel a mixture of the acid **6**, deuterium oxide, cyclohexane, isopropanol and Pt/C as the catalyst. This procedure afforded **6-*d*$_2$** with a deuterium content of 36% (Figure S1). Powdered samples of the pillared metal organic frameworks F_2MOF **1** and F_2MOF **1-*d*$_2$** were prepared under solvothermal conditions by heating a mixture of F_2BDC **6** or **6-*d*$_2$**, DABCO and $Zn(NO_3)_2{\cdot}6H_2O$ in dried DMF at 120 °C for 48 h. The as-synthesized porous material was activated by solvent exchange with dichloromethane and heated at 100 °C under vacuum. The thermal stabilities of F_2MOF **1** and F_2MOF **1-*d*$_2$** were analyzed by thermal gravimetric analysis (TGA). The TGA trace of the as-synthesized material showed a loss of 15% mass from 125 °C to 170 °C that corresponded to DMF (b.p. 152 °C – 154 °C). The material started to decompose at 320 °C (Figure S2). TGA analysis of the activated F_2MOF **1** and F_2MOF **1-*d*$_2$** showed no loss of mass from room temperature to 250 °C. As shown in Figure 2, the experimental powder X-ray diffraction pattern obtained from the activated F_2MOF **1** is in good agreement with those simulated from the published single crystal X-ray diffraction data of isostructural H_4MOF **2** and F_4MOF **3**, as well as that of the tetragonal layered structure of F_2MOF **1** discussed below.

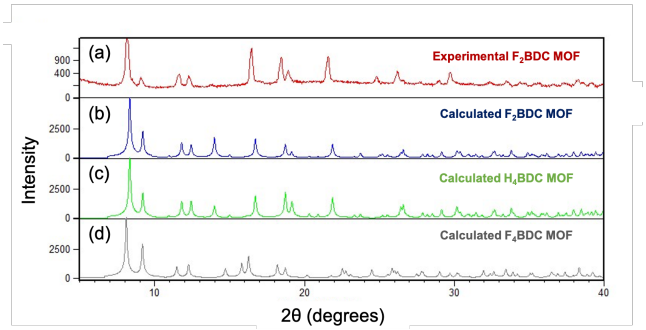

Figure 2. (a) Experimental PXRD pattern from the low temperature phase of F_2MOF **1** compared to those calculated from the single crystal structures of the tetragonal layered structures of: (b) F_2MOF **1**, (c) H_4MOF **2**, and (d) F_4MOF **3**.

Subsequent experiments to obtain diffraction quality single crystals of F_2MOF **1** in dried DMF revealed the formation of two polymorphs depending on crystallization time and temperature. Two different crystalline morphologies were observed using SEM imaging in samples grown at 125 °C and 120 °C (Figure 3). Samples obtained at 120 °C over 24 h consisted of elongated prisms with square or rectangular cross sections (Figure 3a). By contrast, samples synthesized at 125 °C over 12 h contained a mixture of the same prismatic crystals along with various amounts of long needle-like crystals with hexagonal cross sections (Figure 3b).

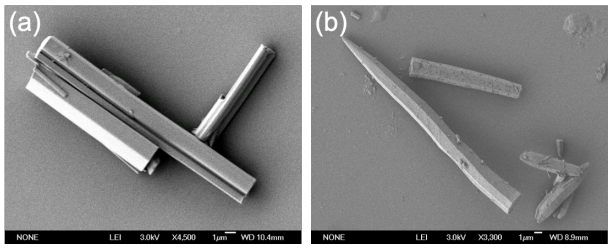

Figure 3. Scanning electron microscopy images of crystals of F_2MOF **1**.

Our attempts to solve the structures of activated samples were successful only for the long needles. The elongated prisms could only be solved in the presence of DMF. Diffraction data were solved, respectively in the hexagonal space group (*P3-*

bar) and in the tetragonal space group (*P4/ncc*) with unit cell parameters of 21.5 x 21.5 x 9.6 Å and 15.0 x 15.0 x 19.2 Å respectively. These structures highlight the well-known framework flexibility of the paddle wheel frameworks (Figure 4).[18] The solvent-free hexagonal structure is characterized by hexagonal channels and triangular units analogous to those found in the framework MIL-68 (Figure 4a).[19] By contrast, the solvent-containing tetragonal network is analogous to that observed with as synthesized H_4BDC MOF **2**, and is characterized by alternating negative and positive radial distortion of the F_2BDC linkers (Figure 4b).[20] The highly disordered solvent molecules could not be modeled accurately and thus were removed using the SQUEEZE algorithm.[21] Taking advantage of the lower temperature synthesis, and using PXRD to confirm the phase identity of our F_2BDC MOF **1** samples (Figure S3), we set out to carry out rotational dynamics and dielectric measurements with samples of the tetragonal solvent-free phase.

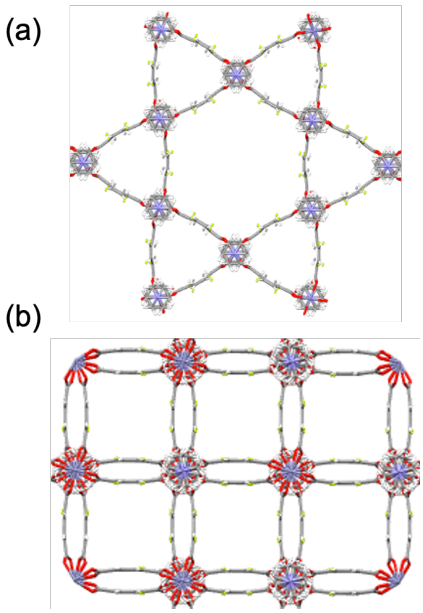

Figure 4. Single crystal X-ray diffraction structures of F_2BDC MOF for (a) hexagonal (*P3-bar*) and (b) tetragonal (*P4/ncc*) polymorphs. X-Ray diffraction data were collected at 100 K.

Solid-State ^{13}C CPMAS NMR Spectroscopy. In agreement with the tetragonal nature of solvent-free F_2MOF **1**, ^{13}C NMR spectra obtained by cross polarization and magic angle spinning (CP-MAS) displayed only five signals (Figure 5). Unique carboxylate (CO) plus fluorinated (C2), quaternary (C1) and protonated (C2) aromatic signals at 167.6, 151.6, 125.6 and 122.9 ppm, respectively. These signals are accompanied by a sharp DABCO peak at ca. 45.9 ppm. A spectrum measured with a short contact time (Figure 5c) to select for carbon atoms linked to hydrogens that have a large heteronuclear dipolar coupling and a fast and efficient cross polarization allowed for the unequivocal assignment of C3 and DABCO. Complementarily, a non-quaternary suppression experiment (NQS) can be used to identify quaternary carbons as well as protonated carbons in groups that experience high mobility (>20 kHz) in the solid state.[22] The spectrum obtained from the NQS experiment (Figure 5a) helps confirm the assignment of the carboxylate (CO), quaternary *ipso*-carbon (C1) and fluorinated C-2 of the F_2BDC linker. Notably, the protonated C3 carbon of the aromatic ring and the methylene carbons of the DABCO linker did not disappear, indicating that both groups experience fast dynamics in the solid state. The assumed symmetry of the crystal requires the position of the fluorine atoms to be rotationally disordered, and the two rotational sites to be crystallographically and magnetically equivalent. In agreement with this expectation, CP-MAS ^{13}C NMR measurements carried out at low temperature, down to 150 K, displayed only insignificant broadening (Figure S4).

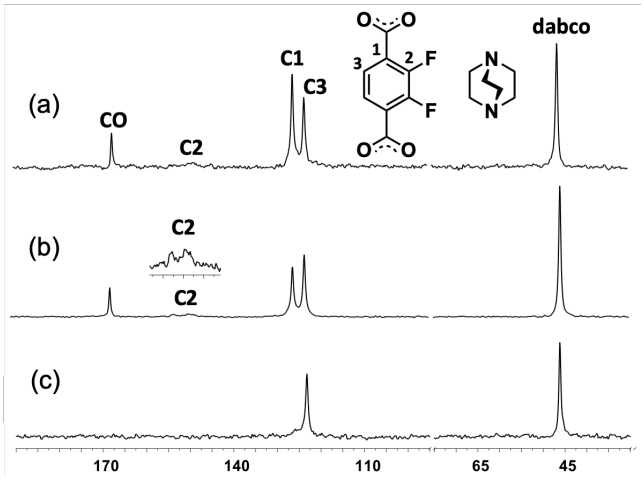

Figure 5. CP MAS ^{13}C NMR of F_2MOF **1**. (a) NQS experiment showing quaternary carbons and protonated carbons of the highly mobile DABCO linker, (b) regular CP-MAS spectrum showing quaternary and protonated carbons and (c) CP-MAS spectrum with a short contact time showing protonated carbons.

Rotational Dynamics by ^{2}H NMR Line-Shape Analysis. With thermal stability data available we set out to investigate the rotational dynamics of the F_2BDC linker in the tetragonal pillared structure of F_2MOF **1**. It has been reported that the rotation of DABCO in pillared MOFs has a low energy barrier,[23] for this reason we did not further investigate its dynamics in F_2MOF **1**. To investigate the dynamics of F_2BDC using solid state NMR, we needed a probe that measures changes in magnetic properties that are not determined by local symmetry and/or changes in chemical shift, but rather by changes in the orientation of F_2BDC rotator with respect to an external frame of reference. A technique that meets this requirement when rotational site exchange dynamics occur in the range of 10^3-10^7 s^{-1} (i.e., 10 kHz to 10 MHz) is quadrupolar echo ^{2}H NMR. The line-shape of the ^{2}H NMR spectrum obtained from powder samples is sensitive to the trajectories and frequencies of motion as the result from the dynamic modulation of the interaction that occurs between electric field gradient and the electric quadrupole moment in the ^{2}H (D) atom.[24] As a result of that, the spectrum changes as a function of the orientation of the C-D bond vector with respect to the orientation of the external magnetic field. With that in mind, a sample of F_2MOF **1** was prepared using the deuterium labeled F_2BDC-d_2 ligand and quadrupolar echo ^{2}H NMR experiments were recorded at 46.2 MHz in the range of 220 to 260 K (Figure 6). The experimental ^{2}H NMR spectra were simulated[25] with a model where the 2,3-difluorophenylene ring reorients by 180° jumps between two equilibrium positions along the 1,4-axis at frequencies that increase as a function of increasing temperature. We found that at 260 K the ^{2}H NMR spectrum line shape is close to the one that has been well documented in the fast exchange regime, in this case ca. 9.7 MHz. With the frequencies of rota-

tion obtained from the simulation of the spectra one can use the Arrhenius equation to calculate an activation barrier of E_a = 6.8±0.1 kcal/mol and an attempt frequency (or pre-exponential factor) of A = 5.4x10^{12} s^{-1}.

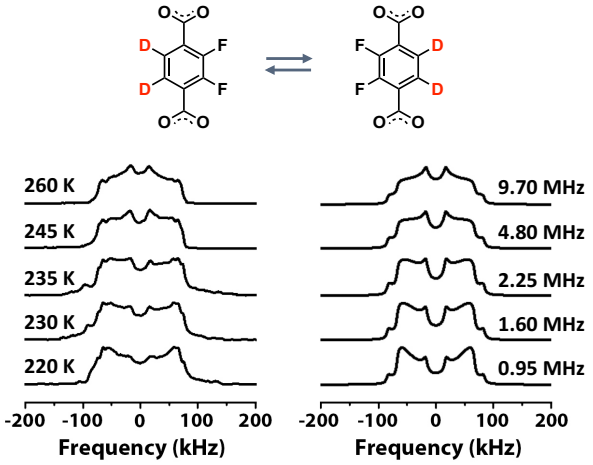

Figure 6. (Left column) Experimental ^{2}H NMR quadrupolar echo spectra, and (right column) spectra simulated assuming rotational trajectories for the phenylene group of 180° jumps with a log-Gauss distribution of activation energies (= 2).

Broadband Dielectric Measurements. Further information about the rotational dynamics for polar molecular rotors can be obtained by frequency and temperature-dependent dielectric measurements, in which the dipolar rotation provides a relaxation mechanism. Figure 7 illustrates the frequency dependence of the real and imaginary parts of the complex dielectric for F_2BDC MOF in the temperature range of 153 – 203 K and the frequency range of 10 Hz to 10 MHz.[26] Changes in the real part of the complex dielectric ( ) are related to the ability of the dipolar rotors in the sample to store electric energy (capacitance) by responding to changes in the direction of the external field. The highest response is observed when the frequency of the external AC field is lower than the characteristic frequency of the rotor. As shown in Figure 7a, an increase in temperature from 153 K to 203 K increases the frequency of the rotational motion k_R and shifts the onset of increased capacitance to higher AC frequency values, . The dotted lines in the Figure represent an ideal Debye relaxation behavior where $_\infty$ and $_s$ are the high frequency and static permittivity, with dipolar rotors having a single rotational time constant $_R$ =1 / k_R.

$$\epsilon' = \epsilon_\infty + \frac{(\epsilon_s - \epsilon_\infty)}{1 + \omega^2 \tau_R^2}$$

On the other hand, an increase in the magnitude of the imaginary part (′) shown in Figure 7b reflects the ability of the material to dissipate energy as the frequency of rotational motion (k_R) and the frequency of the external AC field ( ) approach each other (= k_R).

$$\epsilon'' = \frac{(\epsilon_s - \epsilon_\infty)(\tau_R \omega)}{1 + \omega^2 \tau_R^2}$$

As expected, an increase in temperature shifts the peak to higher frequencies, with each maxima corresponding to the dipolar rotational frequency responsible for the corresponding Debye relaxation. Considering small deviations in Figure 7 between the experimental data points and the simple Debye model, we decided to explore the more complex Cole-Cole[27,28] and Havrilliak-Negami[29] models by plotting the real (ε′) vs. imaginary (ε″) parts of the dielectric constant. In simple terms, it is expected that the data from Debye-type materials with a single relaxation process at a given temperature will result in a perfect semi-circle with deviations observed in the form of flattened

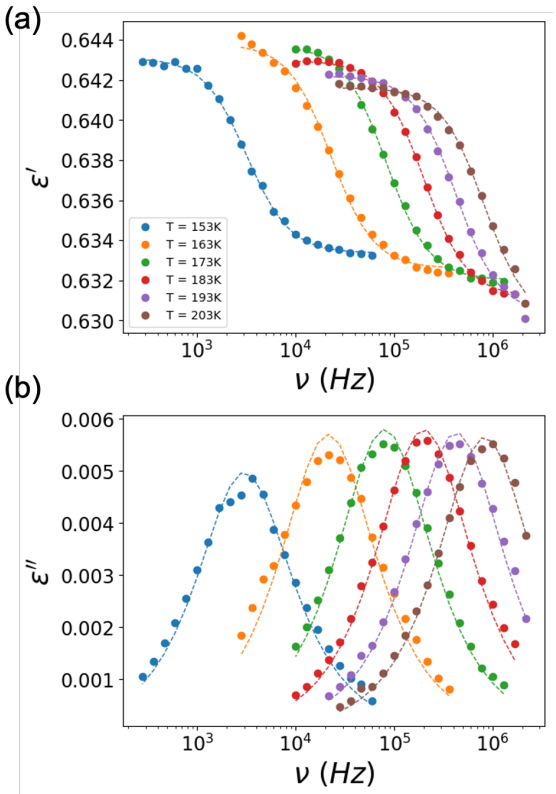

Figure 7. Frequency dependence of (a) the real and (b) imaginary parts of the complex dielectric for F_2BDC MOF crystals in the temperature range of 153 – 203 K.

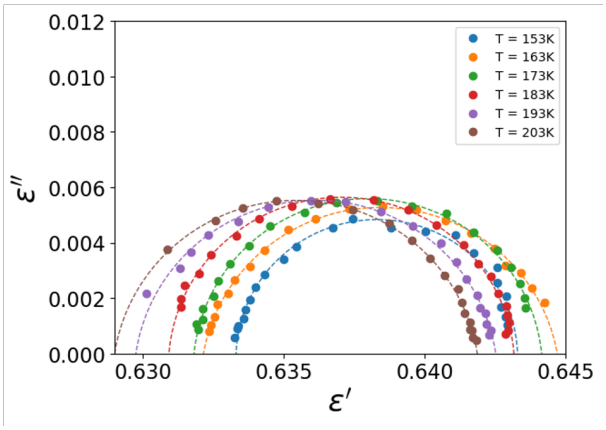

Figure 8. Cole-Cole plot of the real vs. imaginary part of the dielectric constant.

arcs. A plot of ε′ vs. ε″ at different temperatures in Figure 8 shows no significant deviations and fits to the Cole-Cole and Havriliak-Negami models reveal that the broadening and asymmetry parameters are not important – they reduce to the simple Debye model. With that in mind, an Arrhenius plot constructed with the peak relaxation frequency as a function of inverse temperature yields a rotational barrier of 7.1±0.5

kcal/mol and a pre-exponential factor of 1.7×10^{14} s^{-1} (Figure S13), which are in good agreement with those obtained from the VT ^{2}H NMR results.

Computational Analysis. As expected, the activation energy of the dipolar F_2BDC linker in F_2MOF **1** (E_a = 6.8±0.1kcal/mol) is ca. 2.0 kcal/mol lower than that of the non-polar BDC linker (E_a = 8.6±0.5 kcal/mol) in H_4MOF **2**.[14] Considering that F_2MOF **1** and H_4MOF **2** are isostructural, their different barriers heights must relate to relatively small differences that arise from the polar nature of the fluorine atoms and steric effects that arise from their slightly larger size (1.47 Å for F vs 1.20 Å for H). Hoping to determine the contribution of these factors we set out to analyze the rotational potential of F_2BDC using computational methods. A priori, it seemed reasonable that steric and electrostatic interactions between the *ortho*-difluoro substituents and the carboxylate group may destabilize the rotational ground state in the polar F_2BDC and, as suggested in Figure 1, potentially lead to degenerate twisted minima.

The energy scans were carried for a model containing a BDC rotator with Zn-paddle wheel clusters at the ends of the corresponding BDC groups. We built the model based on the atomic coordinates available from the F_2MOF pillared crystal structure. As shown in Figure 9 for F_2MOF **1** (see Figure S16 for H_4MOF **2**), the structure consists of a central BDC bound to two Zn ions at each end. Each Zn dimer is capped with 3 formates and two oppositely disposed ammonia ligands.[30] The coordinates of the zinc cluster acting as a stator were frozen to represent the crystal environment, and only the rotator component with the two carboxylate groups were allowed to relax. The rotational angle was defined as the dihedral between the plane of the two carboxylates and the plane of the aromatic BDC ring, which varied from coplanar (0°, Figure S16a) to orthogonal (90°, Figure S16b). The geometries were optimized and confirmed to be the global minima at DFT level of theory.[31] The barriers to rotation for F_2BDC and BDC rotors were calculated to be 5.3 kcal/mol and 10.9 kcal/mol at the B3LYP-D3/6-311+G(d,p)/LANL2DZ level of theory. These barriers are close to the experimental values of 6.8 kcal/mol and 8.6 kcal/mol for F_2MOF **1** and H_4MOF **2**, respectively.

The F_2BDC rotator was found to have a four-fold symmetric potential characterized by two minima at 0±25.3° and 180±25.3° connected by small maxima that are consistent with a perturbation of the coplanar ground state. Two rotational transition states were identified at 90° and 270° and confirmed by re-optimization using the conventional TS search method. The dihedral angles between the plane of difluorophenylene and the adjacent carbonyl groups were ±5.3° and at ±88.7°, corresponding to nearly co-planar and orthogonal transition state structures (Figure 10b and 10c). The small deviations from 0° and 180° occur in opposite directions for the two carboxylates, and similar deviations were observed in analogous ground state and TS re-optimizations in the case of H_4MOF **2** (Figure S16), where the corresponding angles are 5.1° and 88.7°. This observation suggests an explanation for the lower

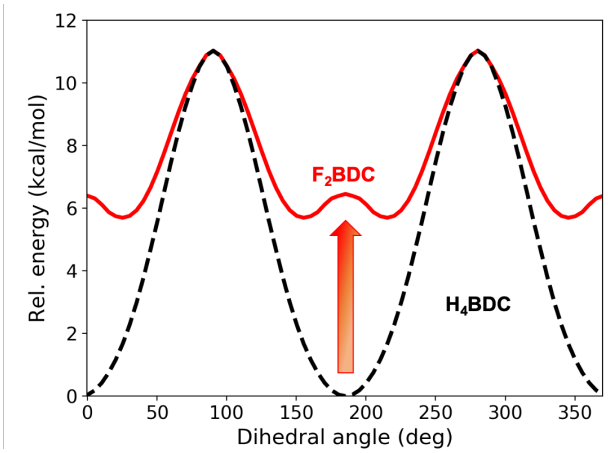

Figure 9. Potential energy for rotation of H_4BDC (black) and F_2BDC (red) at the B3LYP-D3/6-311+G(d,p)/LANL2DZ level of theory.

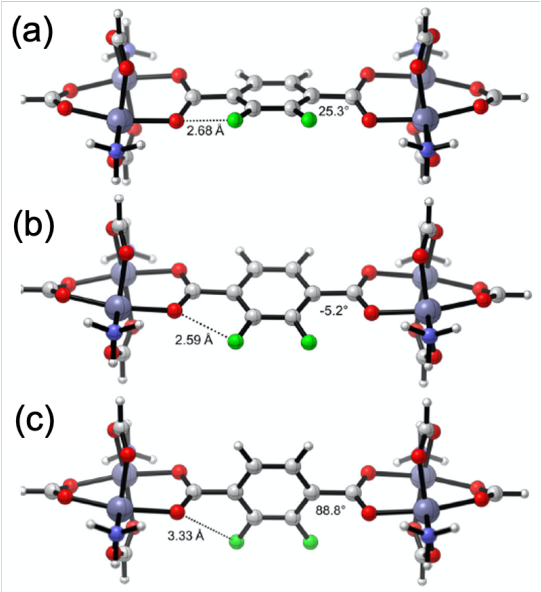

Figure 10. B3LYP-D3/6-311+G(d,p)/LANL2DZ model for the F_2BDC in F_2MOF **1** with structure (a) representing the tilted ground state while structures (b) and (c) represent the planar and orthogonal transition states. The following colors represent atoms: fluorine=green, oxygen=red, hydrogen=white, carbon=grey, nitrogen=blue, zinc=purple.

barrier for the paddle wheel cluster in H_4MOF **2** (8.6 kcal/mol) as compared with that in the zinc oxide cluster in IRMOF-1 (11.3 kcal/mol).[32] We propose that the small bending of the two carboxylates in opposite directions helps avoid a second order saddle point in H_4MOF **2**, reducing the height of the barrier by the observed ca. 3 kcal/mol. The calculated ground state distance between O at the carboxylate and F at the phenylene in Figure 10a was 2.68 Å, which is smaller than the sum of their van der Waals radii of 2.99 Å (1.52 Å for O and 1.47 Å for F). Similarly, distance of 2.42 Å between H and O atoms on the opposite side of the phenylene ring is shorter than the sum of their van der Waals radii of 2.72 Å (1.52 Å for O and 1.2 Å for H), which may lead to weak hydrogen bonding. By contrast, the distance between H and O atoms in the case of the H_4MOF **2** is 2.42 Å (Figure S16). The steric repulsion between the fluorine and oxygen atoms should partially counteract the stabilization provided by hydrogen bonding and

conjugation in the planar species. It is reasonable to conclude that the destabilized ground state is responsible for the lower rotational barrier. On the other hand, the pre-exponential factor for rotation can be viewed as an attempt frequency determined by the torsional mode that described the oscillation of the phenylene group with respect to the plane of the two carboxylates. The calculated frequencies for rotation in the ground state for F_2MOF **1** and H_4MOF **2** are 24.8 cm^{-1} and 40.0 cm^{-1}. These correspond to relatively soft frequencies of $0.74x10^{12}$ s^{-1} and $1.2x10^{12}$ s^{-1}, which are in good agreement with the experimental results.

These computational results are in qualitative agreement with experimental observations reported here and elsewhere. For example, the reported crystal structure of H_4MOF **2** shows the phenylene ring coplanar with the two carboxylates as indicated by the black line H_4BDC potential. While F_2MOF **1** is predicted to have coplanar carboxylate and aromatic groups, it has a lower barrier than **2**, as suggested by the calculations. Similar observations have been made with cubic MOFs $[Zn_4O(XBDC)_3]$, where the unsubstituted phenylene is coplanar with the carboxylate groups[32] while the isoreticular BrBDC[16] (IRMOF-2) and 2-aminophenylene-1,4-dicarboxylate (NH_2BDC)[33] (IRMOF-3) are twisted. The halogenated benzaldehydes have rotational barrier that fall with 7.9±0.2 kcal/mol, while those of halogenated acetophenones fall in the narrow range of 5.5±0.2 kcal/mol.[34] Furthermore, switchable dielectric studies have been reported in plastic crystals,[35] inclusion compounds with rotating guests[36,37] and similar amphidynamic MOF systems.[38] Notably, dielectric relaxation studies of rotatable dipole units were performed in Zr-based MOFs (UiO-66(Zr)) with phenylene rotators functionalized with polar -Br, -2OH, and -NH_2 groups.[38] Switchable dielectric properties were found in UiO-66(Zr)-Br and UiO-66(Zr)-NH_2 systems with rotational barriers of 8.1 kcal/mol and 12.4 kcal/mol, respectively. While the rotational barriers of BrBDC in UiO-66(Zr)-Br and IRMOF-2 architectures are in good agreement, the higher rotational barrier of NH_2BDC in UiO-66(Zr)-NH_2 than in IRMOF-3 was attributed to stronger hydrogen boding in Zr-based MOFs compared to systems with Zn metal nodes. No dielectric response was measured in UiO-66(Zr)-2OH material due to symmetric position of both -OH groups and thus no overall dipole moment. The results from these calculations are consistent with the suggestion that rotators with *ortho* groups have a lower barrier, at least in part, as the result of steric and electrostatic destabilization of the co-planar ground state.

CONCLUSIONS

We report the synthesis, characterization, and rotational dynamics of F_2MOF **1** featuring the dipolar 2,3-difluorophenylene ligand (F_2BDC), which was expected to have a relatively low barrier as a result of ground state destabilization. We have previously shown that a rotational barrier in amphidynamic crystals could be controlled via their structural features such as inserting rotators within various axle topologies or choosing rotators with globular shapes and a high rotational symmetry order. This study establishes a new strategy for rotational barrier control via the ground state destabilization and showcases the promise of polar phenylenes in the design of dipolar rotor arrays where dipole-dipole interactions are greater than the structural barriers ($E_{DD} >> kT \geq Ea$). The pillared structure of F_2MOF **1** was confirmed by single crystal and powder XRD, which was in good agreement to the ones reported for H_4MOF **2** and the isostructural analog F_4MOF **3**. The rotational dynamics of the F_2BDC linker studied by VT quadrupolar echo ^{2}H NMR and dielectric spectroscopy revealed an activation energy E_a = 6.8±0.1 kcal/mol and E_a = 7.1 ± 0.5 kcal/mol that is ca. 2 kcal/mol lower than that of H_4MOF **2** (8.6±0.5 kcal/mol). Dielectric response measurements revealed a single relaxation Debye-type behavior as a result of the rotational behavior of the dipolar F_2BDC linker. Potential energy calculations at different rotation angles at the B3LYP-D3/6-311+G(d,p)/LANL2DZ level of theory confirmed the expected destabilization of the ground state in F_2MOF **1** and matched the experiment reasonably well with barrier of 5.3 kcal/mol. A pre-exponential factor A = $5.4x10^{12}$ s^{-1} obtained from the experiment was also approximated well by the calculated frequency of the torsional mode determined by the plane of the difluorophenylene rotator with respect to the framework carboxylates ($0.74x10^{12}$ s^{-1}). Given the growing interest in understanding the main principles in molecular machine design through a structure-energy relationship, this study shows progress toward the engineering of polar rotators with a low barrier in the crystalline solid state.

ASSOCIATED CONTENT

Supporting Information

Synthesis and characterization of ligands **6** and **6-*d*$_2$** and F_2MOF **1** and **1-*d*$_2$**. Characterization procedures: solution ^{1}H and ^{13}C NMR, IR, Powder X-ray diffraction, TGA, CP-MAS ^{13}C NMR solid state quadrupolar echo ^{2}H NMR (PDF). Single-crystal X-ray structures for F_2MOF **1** are available as CIF and were also deposited as CCDC 2003820-2003821**.** Computational details. This Information is available free of charge on the ACS Publications website at DOI.

AUTHOR INFORMATION

Corresponding Author

* E-mail: mgg@chem.ucla.edu

Funding Sources

National Science Foundation grants NSF DMR 1700471 to MGG and NSF CHE 1764328 to KNH. Solid state NMR measurements were carried out with an instrument obtained with support from grant MRI 1532232. Computations were performed on the Hoffman2 cluster at UCLA and the Extreme Science and Engineering Discovery Environment (XSEDE), which is supported by the NSF (OCI-1053575). CMH research was supported by the UCLA-DOE Center for Global Mentoring.

ACKNOWLEDGMENT

This work was supported by National Science Foundation grants DMR 1700471 and solid state NMR measurements were carried out with an instrument obtained with support from grant MRI 1532232. Dielectric measurements were conducted at the Oak Ridge National Laboratory's Center for Nanophase Materials Sciences, which is a DOE Office of Science User Facility.

REFERENCES

(1) Khuong, T. A.; Nunez, J. E.; Godinez, C. E.; Garcia-Garibay, M. A. Crystalline molecular machines: A quest toward solid-state dynamics and function. *Acc. Chem. Res.* **2006**, *39*, 413–422.

(2) Garcia-Garibay, M. A. Crystalline molecular machines: Encoding supramolecular dynamics into molecular structure. *Proc. Natl. Acad. Sci. U. S. A.* **2005**, *102*, 10771–10776.

(3) Vogelsberg, C. S.; Garcia-Garibay, M. A. Crystalline molecular machines: function, phase order, dimensionality, and composition. *Chem. Soc. Rev.* **2012**, *41*, 1892–1910.

(4) Howe, M. E.; Garcia-Garibay, M. A. The Roles of Intrinsic Barriers and Crystal Fluidity in Determining the Dynamics of Crystalline Molecular Rotors and Molecular Machines. *J. Org. Chem.* **2019**, *84*, 9835–9849.

(5) Akutagawa, T.; Koshinaka, H.; Sato, D.; Takeda, S.; Noro, S.-I.; Takahashi, H.; Kumai, R.; Tokura, Y.; Nakamura, T. Ferroelectricity and polarity control in solid-state flip-flop supramolecular rotators. *Nat. Mater.* **2009**, *8*, 342–347.

(6) Comotti, A.; Bracco, S.; Yamamoto, A.; Beretta, M.; Hirukawa, T.; Tohnai, N.; Miyata, M.; Sozzani, P. Engineering switchable rotors in molecular crystals with open porosity. *J. Am. Chem. Soc.* **2014**, *136*, 618–621.

(7) Setaka, W.; Yamaguchi, K. Thermal modulation of birefringence observed in a crystalline molecular gyrotop. *Proc. Natl. Acad. Sci. U. S. A.* **2012**, *109*, 9271–9275.

(8) Setaka, W.; Yamaguchi, K. A Molecular Balloon: Expansion of a Molecular Gyrotop Cage Due to Rotation of the Phenylene Rotor. *J. Am. Chem. Soc.* **2012**, *134*, 12458–12461.

(9) Kottas, G. S.; Clarke, L. I.; Horinek, D.; Michl, J. Artificial molecular rotors. *Chem. Rev.* **2005**, *105*, 1281–1376.

(10) Garcia-Garibay, M. A. Molecular machines: nanoscale gadgets. *Nat. Mater.* **2008**, *7*, 431–432.

(11) Erbas-Cakmak, S.; Leigh, D. A.; McTernan, C. T.; Nussbaumer, A. L. Artificial molecular machines. *Chem. Rev.* **2015**, *115*, 10081–10206.

(12) Horansky, R. D.; Clarke, L.I.; Price, J. C.; Khuong, T.-A. V.; Jarowski, P. D.; Garcia-Garibay, M. A. Dielectric response of a dipolar molecular rotor crystal. *Phys. Rev. B.* **2005**, *72*, No. 014302.

(13) Horansky, R. D.; Clarke, L. I.; Winston, E. B.; Price, J. C.; Karlen, S. D.; Jarowski, P. D.; Santillan, R.; Garcia-Garibay, M. A. Dipolar rotor-rotor interactions in a difluorobenzene molecular rotor crystal. *Phys. Rev. B* **2006**, *74*, No. 054306.

(14) Khudozhitkov, A. E.; Kolokolov, D. I.; Stepanov, A. G.; Bolotov, V. A.; Dybtsev, D. N. Metal-Cation-Independent Dynamics of Phenylene Ring in Microporous MOFs: A ^{2}H Solid-State NMR Study. *J. Phys. Chem. C* **2015**, *119*, 28038–28045.

(15) Chun, H.; Dybtsev, D. N.; Kim, H.; Kim, K. Synthesis, X-ray Crystal Structures, and Gas Sorption Properties of Pillared Square Grid Nets Based on Paddle-Wheel Motifs: Implications for Hydrogen Storage in Porous Materials. *Chem. Eur. J.* **2005**, *11*, 3521–3529.

(16) Winston, E. B.; Lowell, P. J.; Vacek, J.; Chocholousova, J.; Michl, J.; Price, J. C. Dipolar molecular rotors in the metal-organic framework crystal IRMOF-2. *Phys. Chem. Chem. Phys.* **2008**, 10, 5188−5191.

(17) Analogous observations and computational analyses have been made with 1,4-naphthalene dicarboxylate: Amirjalayer, S.; Schmid, R. Conformational Isomerism in the Isoreticular Metal Organic Framework Family: A Force Field Investigation. *J. Phys. Chem. C* **2008**, *112*, 14980–14987.

(18) Schneemann, A.; Bon, V.; Schwedler, I.; Senkovska, I.; Kaskel, S.; Fischer, R. A. Flexible metal–organic frameworks, *Chem. Soc. Rev.,* **2014**, *43*, 6062–6096.

(19) Barthelet, K.; Marrot, J.; Ferey, G.; Riou, D. $V^{III}(OH)\{O_2C–C_6H_4–CO_2\}.(HO_2C–C_6H_4–CO_2H)_x(DMF)_y(H_2O)_z$ (or MIL-68), a new vanadocarboxylate with a large pore hybrid topology: reticular synthesis with infinite inorganic building blocks? *Chem. Commun.* **2004**, 520–521.

(20) Dybtsev, D. N.; Chun, H.; Kim, K. Rigid and Flexible: A Highly Porous Metal-Organic Framework with Unusual Guest-Dependent Dynamic Behavior. *Angew. Chem. Int. Ed.* **2004**, *43*, 5033–5036.

(21) Spek, A. Structure validation in chemical crystallography. *Acta Crystallogr., Sect. D: Biol. Crystallogr.* **2009**, *65*, 148–155.

(22) Alemany, L. B.; Grant, D.M.; Alger, T.D.; Pugmire, R. J. Cross polarization and magic angle sample spinning NMR spectra of model organic compounds. 3. Effect of the carbon-13-proton dipolar interaction on cross polarization and carbon-proton dephasing *J. Am. Chem. Soc.* **1983**, *105*, 6697–6704

(23) Burtch, N. C.; Torres-Knoop, A.; Foo, G. S.; Leisen, J.; Sievers, C.; Ensing, B.; Dubbeldam, D.; Walton, K. S. Understanding DABCO nanorotor dynamics in isostructural metal-organic framework. *J. Phys. Chem. Lett.* **2015**, *6*, 812–816.

(24) Fyfe, C. A. *Solid State NMR for Chemists;* CFC Press: Guelph, Ontario, 1983.

(25) Macho, V.; Brombacher, L.; Spiess, H. W. The NMR-WEBLAB: an Internet Approach to NMR Lineshape Analysis. *Appl. Magn. Reson.* **2001**, *20*, 405–432.

(26) The F$_i$MOF crystalline sample was measured in the powder form. Unlike liquids, powdery samples by definition do not fill up the entire cell. As a result, the absolute value of permittivity does not mean much. For this type of material, we would not expect the real permittivity to be smaller than one. However, because of the powdery nature of the sample, the apparent real permittivity, which is calculated according to the nominal geometry of the cell, becomes less than one.

(27) Cole K. S.; Cole R. H. Dispersion and absorption in dielectrics I. Alternating current characteristics. *J. Chem. Phys.* **1941**, *9*, 341–349.

(28) Cole K. S.; Cole R. H. Dispersion and absorption in dielectrics II. Direct current characteristics. *J. Chem. Phys.* **1942**, *10*, 98–105

(29) Havriliak, S.; Negami, S. A complex plane representation of dielectric and mechanical relaxation processes in some polymers. *Polymer* **1967**, *8*, 161–210.

(30) Pakhira, S.; Takayanagi, M.; Nagaoka, M. Diverse Rotational Flexibility of Substituted Dicarboxylate Ligands in Functional Porous Coordination Polymers. *J. Phys. Chem. C* **2015**, *119*, 28789–28799.

(31) Frisch, M. J.; Trucks, G. W.; Schlegel, H. B.; Scuseria, G. E.; Robb, M. A.; Cheeseman, J. R.; Scalmani, G.; Barone, V.; Mennucci, B.; Petersson, G. A.; et al. Gaussian 09; Gaussian, Inc, Wallingford, CT, 2013.

(32) Gould, S. L.; Tranchemontagne, D.; Yaghi, O. M.; Garcia-Garibay, M. A. Amphidynamic character of crystalline MOF-5: Rotational dynamics of terephthalate phenylenes in a free-volume, sterically unhindered environment. *J. Am. Chem. Soc.* **2008**, *130*, 3246–3247.

(33) Morris, W.; Taylor, R. E.; Dybowski, C.; Yaghi, O. M.; Garcia-Garibay, M. A. Framework mobility in the metal-organic framework crystal IRMOF-3: Evidence for aromatic ring and amine rotation. *J. Mol. Struct.* **2011**, *1004*, 94–101.

(34) Drakenber, T.; Sommer, J. The torsional barrier in aromatic carbonyl compounds, *J. Chem. Soc. Perkins II* **1980**, 363–369.

(35) Sun, Y.-Z.; Huang, B.; Xu, W.-J.; Zhou, D.-D.; Chen, S.-L.; Zhang, S.-Y.; Du, Z.-Y.; Xie, Y.-R.; He, C.-T.; Zhang, W.-X., et al. Plastic Crystals with Polar Halochromate Anion: Thermosensitive Dielectrics Based upon Plastic Transition and Dipole Rotation. *Inorg. Chem.* **2016**, *55*, 11418–11425.

(36) Zeng, Y.; Huang, R.-K.; Du, Z.-Y.; He, C.-T.; Zhang, W.-X.; Chen, X.-M. Matching of Host−Guest Symmetry/Orientation and Molecular Dynamics in Two Double Perovskite-Like Azido Coordination Polymers. *Inorg. Chem.* **2017**, *56*, 9946–9953.

(37) Zhang, W.; Ye, H.-Y.; Graf, R.; Spiess, H. W.; Yao, Y.-F.; Zhu, R.-Q.; Xiong, R.-G. Tunable and Switchable Dielectric Constant in an Amphidynamic Crystal. *J. Am. Chem. Soc.* **2013**, *135*, 5230–5233.

(38) Devautour-Vinot, S.; Maurin, G.; Serre, C.; Horcajada, P.; da Cunha, D. P.; Guillerm, V.; de Souza Costa, E.; Taulelle, F.; Martineau, C. Structure and Dynamics of the Functionalized MOF Type UiO-66(Zr): NMR and Dielectric Relaxation Spectroscopies Coupled with DFT Calculations. *Chem. Mater.* **2012**, *24*, 2168–2177.

TOC Graphic